ISSN 2504-9593
DOI: 10.5281/zenodo.20191778
https://ijree.com/index.php/publications/article/view/42
Int. J. Renew. Energ & Environ Vol.4 (2), pp 27-44(2026)

UTILIZATION OF BIOWASTE (*Allium cepa L* PEEL EXTRACT) FOR THE SYNTHESIS OF MgO-NPs FOR THEIR ENERGY HARVESTING POTENTIALS

[1*]Okhuarobo, L.O., [2]Iyasele, J. U., [3]Elemike, E. E., [1]Akpeji, B.H.

[1]Department of Science Laboratory Technology, Federal University of Petroleum Resources, Effurun, Delta State.
[2]Department of Chemistry, University of Benin Edo State, Nigeria.
[3]Department of Chemistry, Federal University of Petroleum Resources, Effurun, Delta State.
Corresponding author: **E-mail:** okhuarobo.osamwen@fupre.edu.ng **Tel:** +2348037343031

Abstract
The synthesis of Magnesium oxide nanoparticles (MgO-NPs) with the use of Allium cepa L (onion) peel waste is a promising alternative to traditional chemical methods. The Allium cepa L peel extract was used as a substrate for the synthesis of MgO-NPs using bottom-up approach. The extract phytochemically screened, demonstrated the presence of saponins, alkaloids, flavonoids, phenolics, and other bioactive compounds, which enhance and act as a bio-reductants to MgO-NPs formation. The biosynthesized MgO-NPs were investigated for optical properties, functional moieties, crystallinity state, elemental constituents, morphology, particle size and their energy harvesting abilities using UV-Visible spectrophotometry, Fourier Transform Infrared Spectrophotometry (FTIR), Energy Dispersive Spectrometry (EDX), Transmission Electron Microscopy (TEM), Scanning electron microscopy (SEM) and Tauc's plot respectively. UV-Visible spectrum revealed that MgO-NPs showed maximum absorption at wavelength of 241nm in the ultraviolet region. FTIR results showed prominent peaks at 3464cm^{-1}, 3360cm^{-1} represents stretching vibration of O-H group. The peaks at 1592cm^{-1}, 1171 cm^{-1} represents the stretching vibration of aromatic C=C bond. EDX results revealed the elemental composition in percentages of the elements in the nanoparticles, showing Mg (69.96%, 3.85 keV), O (26.67 %, 1.09 keV) and C (8.34 %, 1.26 keV). PXRD revealed a crystalline, cubid shaped with porous surface for SEM. The particle size (average) of the nanoparticles as characterized by TEM were found to be 63 nm. The band gap energy was calculated using Tauc's plot to be 3.57 eV.
Keywords: Green synthesis, biowaste utilization, MgO nanoparticles, *Allium cepa*, biowaste utilization, energy harvesting.

1.0 INTRODUCTION

The rapid advancement in nanotechnology has led to an increased demand for metal oxide nanomaterials due to their unique properties and diverse applications in electronics, energy, catalysis and environmental remediation. Among various metal oxides, magnesium oxide nanoparticles (MgO-NPs) have gained significant attention in energy applications due to their unique physicochemical properties, including wide bandgap, high thermal stability, excellent optical properties and remarkable catalytic activity (Ahn *et al*., 2018; Kumar *et al.,* 2020). However, conventional synthesis methods for MgO-NPs often involve hazardous chemicals, high energy consumption, and generate toxic bye-product, contradicting the principles of green chemistry and sustainable development (Nasrollahzadeh *et al.,* 2019). The chlorophyll molecule ($C_{55}H_{72}O_5N_4Mg$), which is essential in absorbing light energy during photosynthesis, contains magnesium as a key

component as shown in figure 1 below. The emerging shift toward green synthesis methodologies has gained significant momentum, with biological systems offering environmentally benign alternatives for nanoparticle synthesis (Ituen and Archibong, 2022). Plant-mediated synthesis, in particular, has attracted considerable attention due to the abundance of bioactive compounds that serve as natural reducing agents, stabilizers, and capping agents (Singh *et al.,* 2018). Among various plant materials, agricultural waste represents an untapped resource that can simultaneously address waste management challenges while providing cost-effective precursors for nanomaterial synthesis (Singh *et al.,* 2023).

Allium cepa L (onion) is an extensively cultivated and consumed vegetables worldwide, with global production exceeding 100 million tonnes annually (FAOSTAT, 2023). The processing and consumption of onions generate substantial quantities of peel waste, estimated at 10-15% of the total weight, which is typically discarded or used for low-value applications such as composting (Ituen *et al.,* 2020). Onion peels are rich repositories of bioactive compounds, including flavonoids (quercetin, kaempferol), phenolic acids (ferulic acid, caffeic acid), anthocyanins, and organosulfur compounds, which possess strong antioxidant and reducing properties (Sharma *et al.,* 2015). Despite the growing interest in green synthesis of metal oxide nanmomaterials, comprehensive studies on utilization of onion peel extract for MgO-NP synthesis and their systematic evaluation for energy harvesting applications remain limited (Ituen and Archibong, 2022, Roy *et al.,* 2021, Pathak *et al.,* 2019). Previous researches have primarily focused on antimicrobial and biomedical applications (Ikhioya *et al.,* 2023).

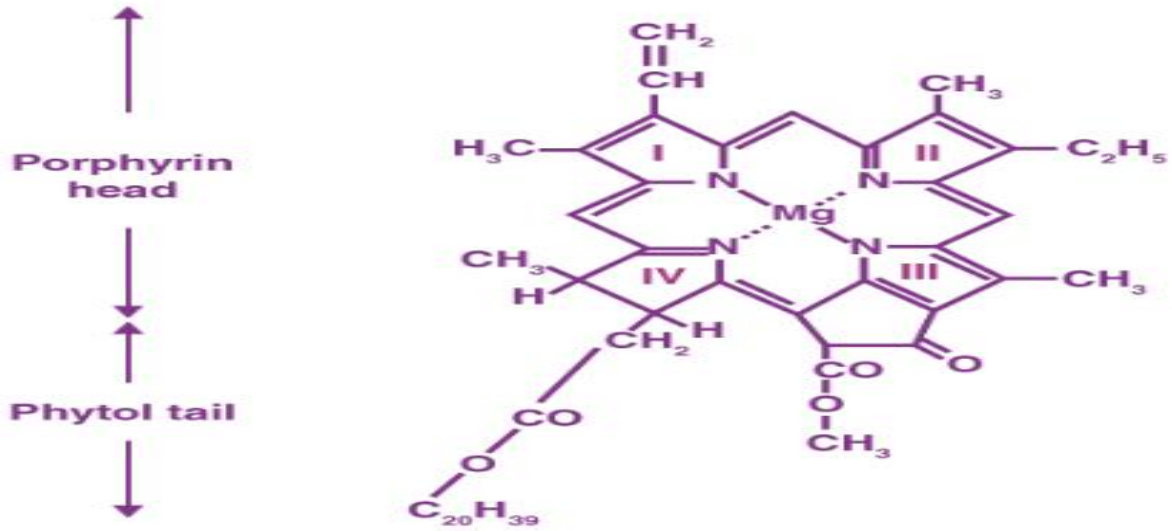

Figure 1: Structure of Chlorophyll (Sharma *et al.,* 2015)

This study addresses these knowledge gaps by developing a novel, sustainable synthesis route for MgO-NPs using *Allium cepa* peel extract and conducting evaluation of their energy harvesting potential. The research objectives include: The extraction of the bioactive component from *Allium cepa L* peel by maceration method, qualitatively determine

Phytochemical Properties of the aqueous extract of onion peel, synthesize MgO-NPs, determine the energy band gap of MgO-NPs using Tauc`s plot and to determine the electrochemical properties of the synthesized MgO-NPs using its energy band gap.

2.0 MATERIALS AND METHODS

Formation of MgO-NPs and absorption wavelength were determined by UV-Vis spectroscopy (UV-2600 Spectrophotometer). X-ray diffraction (XRD) spectroscopy at 2θ = 10^{o} – 80^{o} in comparison with the extract and Energy dispersive X-ray spectroscopy (EDS, EVO MA 15 Zeiss). The morphology of the MgO-NPs and size was characterized by transmission electron microscopy (TEM, FEI TECHNAI G2F20). Fourier transform infrared (FTIR) spectroscopy were used to determine functionalities within 400 - 4500 cm^{-1} using a PerkinElmer spectrophotometer (Beijing Rayleigh). The current-voltage responses and photoelectrochemical properties were determined at one sun illumination (AM 1.5 G, 100 $mWcm^{-2}$) using a Keithley 2400 source measurement unit and by electrochemical impedance spectroscopy (EIS, Gamry REF600 workstation).

2.1.0 Methods

2.1.1 Collection and Extraction of *Allium cepa* L Peel Extract (Ikhuoria *et al*., 2024)

Fresh onions (*Allium cepa* L) were purchased from Hausa Market in Warri-Sapele Road, Uvwie LGA, Delta State, Nigeria and taxonomically authenticated at the Department of Plant Biology and Biotechnology, University of Benin., Nigeria. The Magnesium precursors, specifically Magnesium acetate tetrahydrate $(CH_3COO)_2Mg\cdot 4H_2O$) and Sodium hydroxide (NaOH) was purchased from Winteck Nig Ltd (Sigma-Aldrich Product). The *Allium cepa L* Peel (100 g) were rinsed with distilled water to remove impurities and air-dried at room temperature for 48 hours. The dried peels were ground into fine powder using a mechanical grinder. The powdered peel (20g) was boiled in 100 mL of distilled water at 70°C for 2 hours under continuous stirring. The resulting solution was cooled to room temperature and filtered through Whatman filter paper. The filtrate was stored at 4°C

2.2. Phytochemical and Bioactive Components of aqueous Extract of *Allium cepa* L Peel

A number of phytochemicals in the aqueous extract of *Allium cepa* L Peel were identified using the procedure mentioned by (Akpeji *et al.,* 2024a; Ikhuoria *et al*., 2024). Figure 2: Shows flow diagram describing the process of extraction.

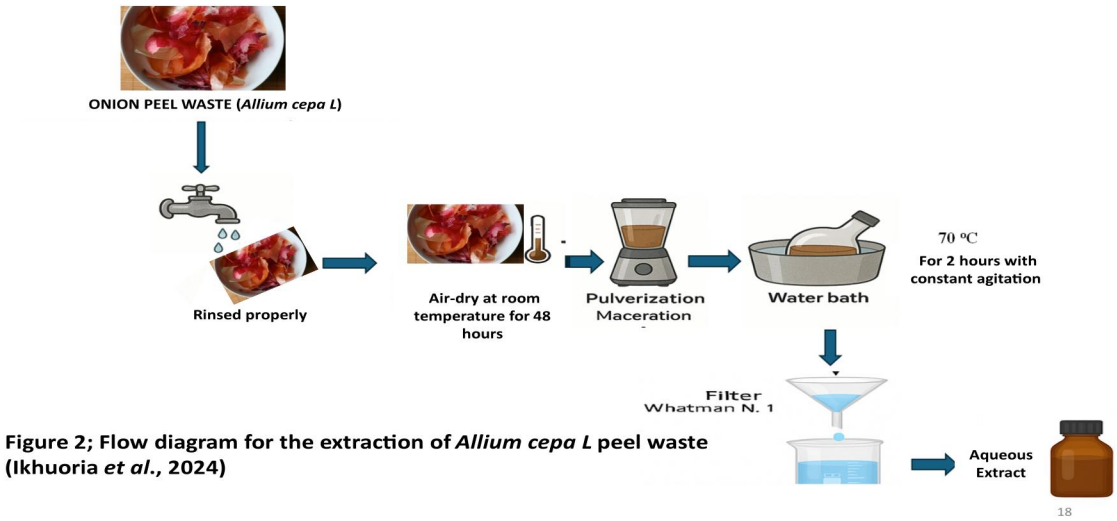

Figure 2; Flow diagram for the extraction of *Allium cepa L* peel waste (Ikhuoria *et al.*, 2024)

18

2.3. Phytochemical and Bioactive Components of aqueous Extract of *Allium cepa L* peel

A number of phytochemicals in the aqueous extract of *Allium cepa L* peel were identified using the procedure according to (Akpeji *et al.,* 2024a; Akpeji *et al.,* 2024b; Akpeji and Singh, 2026; Ikhuoria *et al*., 2024; Odeja *et al.,* 2026) but with slight modification.

2.3.1 Alkaloid Test (Wagner's test): Alkaloids give reddish brown precipitate with Wagner's reagent. (Solution of iodine in potassium iodide)..

2.3.2 Reducing Sugars: A volume of about 2 mL of aqueous extract *Allium cepa L* peel was placed in the test tube, to which Benedict reagent was added after which the contents were warmed gently. Presence of red precipitate in the test tube proves that at least some reducing sugars were originally present in the *Allium cepa L* peel extracts.

2.3.3 Saponin test: 5mL of distilled water were added to 2mL of the *Allium cepa L* peel extracts in the testube. It was shaken very vigorously. The presence of saponin was proven when compact, continuous and well formed froth is maintained approximately after 2 minutes.

2.3.4 Phenolic Compound test (ferric chloride test): Few drops of 10 percent ferric chloride solution was added to 2mL of the aqueous extract of *Allium cepa L* peel. The colouration of the green-blue that is the indicator to the presence of the phenolic compounds.

2.3.5 Carbohydrates test: Correctly, 5mL of Fehling solution was added to 2mL of aqueous extract mixture and then left to boil on water bath. The presence of carbohydrate was also observed because the production of yellow precipitate was also observed.

2.3.6 Test of tannins: To 2mL of the *Allium cepa L* peel extracts, 50 percent ferric chloride solution was added and the formation of a dark green precipitate confirmed that the peel had tannins.

2.3.7 Test of flavonoids: 2 mL of the aqueous extract of *Allium cepa L* peel, we added a small portion of water, then we added several drops of the lead acetate solution in which a light yellow precipitate that indicates the flavonoid compound was produced.

2.3.8 Steroids: The Liebermann Burchard test was carried out on steroids. Chloroform was then added to the *Allium cepa L* peel extracts then acetic anhydride and concentrated sulfuric acid. Steroids were present with a blue-green coloration was formed.

2.3.9 Test for saponins (froth test): 5 ml of extract was boiled in 10 ml distilled water in a test tube and was shaken vigorously for about 30 seconds. The test tube was allowed to settle for half an hour, formation of froth indicated the presence of saponins.

2.4 Bio-synthesis of MgO-NPs from aqueous extract of *Allium cepa L* peel

MgO-NPs were synthesized using the green synthesis approach. A 0.1 M solution of $(CH_3COO)_2Mg\cdot 4H_2O$ was prepared with distilled water. The *Allium cepa L* peel extract (10 mL) was added dropwise to 100mL of the magnesium acetate solution under continuous stirring at room temperature. The pH of the solution was adjusted to 12 using 1 M NaOH solution. The mixture was heated at 80°C for 3 hours with constant stirring. A white precipitate formed during this process, indicating the formation of MgO-NPs. The precipitate was collected by centrifugation at 6000 rpm for 15 minutes, washed multiple times with distilled water and oven dried at 80°C for 2 hours. The procedure and mechanism is as presented in figure 4 and its reaction in equation 1.

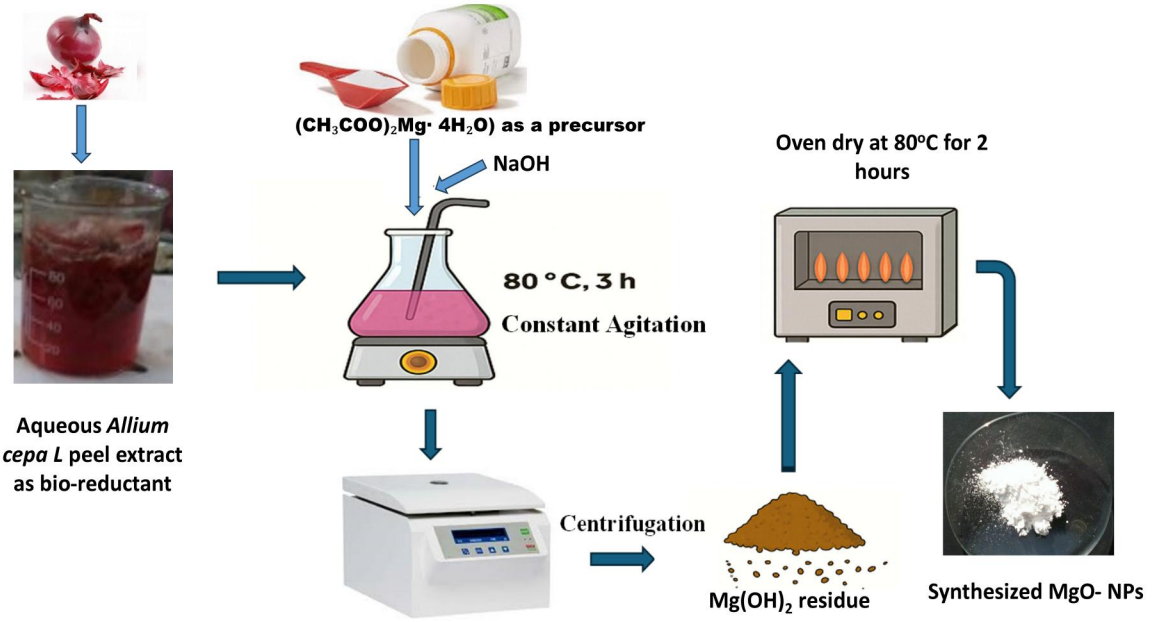

$[Mg(CH_3COO)_2.\ xH_2O]$ + (Phyto-metabolites) + NaOH → $Mg(OH)_2$ + drying to remove H_2O → MgO-NPs ⟶ equation 1

Figure 3. Green Synthesis of MgO -NPs (Ikhuoria *et al.*, 2024)

20

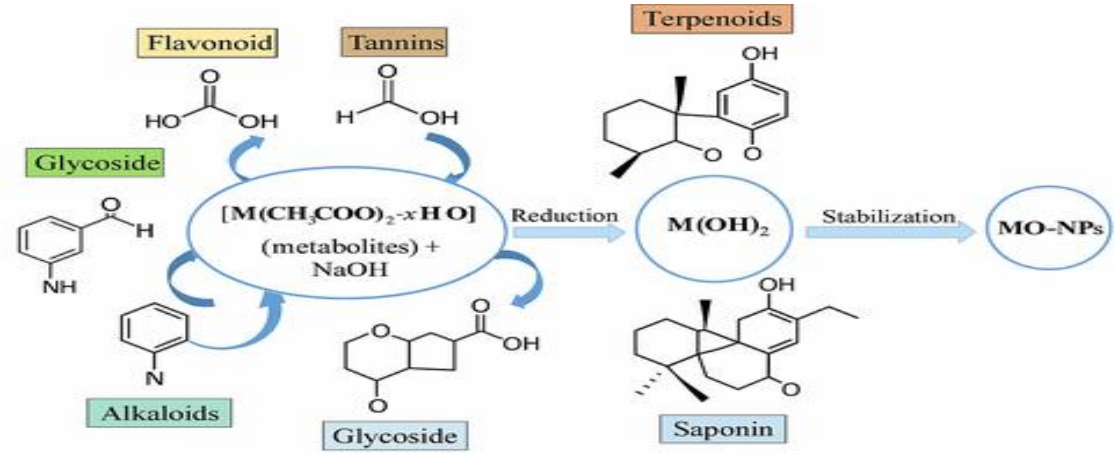

Figure 4: Mechanism of bio-reduction of $(CH_3COO)_2Mg\cdot 4H_2O$ into MgO-NPs using *Allium cepa L* peel, modified from (Akpeji *et al.*, 2024a). M = Mg

3.0 Characterization Techniques

The synthesized MgO-NPs were characterized using multiple analytical techniques:

3.1 X-ray Diffraction (XRD): Crystal structure analysis was performed using a Rigaku MiniFlex 600 diffractometer equipped with Cu Kα radiation (λ = 1.5406 Å). Diffraction patterns were recorded in the 2θ range of 10-80° with a step size of 0.02° and counting time of 1 s per step. Phase identification was conducted using the International Centre for Diffraction Data (ICDD) database, and crystallite size was calculated using the Debye-Scherrer equation.

3.2 Field Emission Scanning Electron Microscopy (FE-SEM): Morphological analysis was conducted using a JEOL JSM-7610F field emission scanning electron microscope operated at 5-15 kV accelerating voltage. Samples were sputter-coated with a thin layer of gold to enhance conductivity and prevent charging effects.

3.3 High-Resolution Transmission Electron Microscopy (HR-TEM): Detailed structural analysis was performed using a JEOL JEM-2100F transmission electron microscope operated at 200 kV. Samples were prepared by dispersing synthesized nanoparticles in ethanol and dropping the suspension onto carbon-coated copper grids.

3.4 Fourier Transform Infra-red Spectroscopy (FTIR): Functional group analysis was conducted using a PerkinElmer Spectrum Two FTIR spectrometer equipped with a universal ATR accessory. Spectra recorded in the range of 400-4000 cm^{-1} with a resolution of 4 cm^{-1} and 32 scans per measurement.

3.5 UV-Visible Spectroscopy: Optical properties were investigated using a Shimadzu UV-3600 Plus spectrophotometer in the wavelength range of 200-800 nm. Bandgap energy was determined from the Tauc's plot analysis of the absorption data.

4.0 RESULTS AND DISCUSSION

4.1 Phytochemical analysis of aqueous extract *Allium cepa L* peel

The phytochemical composition of the *Allium cepa L* peel extract revealed essential information on how well the waste works as a reaction media to create MgO NPs in the green synthesis as well as an impact on the electrochemical properties of the synthesized

nanomaterial. The brown liquid-like extract showed positive tests on various bioactive chemical compounds such as saponins, phenolic, carbohydrates, tannins, flavonoids, and glycosides following the previous report obtained by (Ahmed *et al.,* 2016; Akpeji *et al.,* 2024b Okewale and Akpeji, 2022; Okewale *et al.,* 2019). These phytometabolites synergistically involved in the formation of nanoparticles, leading to metal ion reduction, stability of formed particles, and functionalization of the particles surface, which enhance the electrochemical efficiency capabilities of the MgO-NPs (Gurunathan *et al*., 2020; Akpeji *et al.,* 2024a).

The *Allium cepa L* peel extract contains saponin as shown in table 1: saponin is a natural surfactant since it has amphiphilic molecules. They allow uniform nucleation and controlled nucleation of MgO-NPs by reducing agglomeration and colloidal stability. When applied to an electrochemical system, such structural uniformity equates to a better electrode surface area and more unified ionic pathways, which is critical towards the increase of charge harvesting (Roy *et al*., 2021; Akpeji and singh, 2026).

Moreover, saponins help to enhance the mechanical integrity of the electrode coating, and thus result in cyclic stability in capacitors. The extract also displayed the presence of alkaloids, that is, heterocyclic rings bearing nitrogen. The compounds also allow reducing Mg^{2+} and can also introduce nitrogen groups to the surface of MgO-NPs simultaneously, acting as electron donors to reduction processes. It has been documented that nitrogen-doping helps to alter the electrical conductivity and electrochemical sensitivity of metal oxides (Patil *et al*., 2022; Ogwuche *et al.,* 2023). When applied to energy it enables faster electron transfer, greater charge capacity and lower internal resistances in electrodes made of biosynthesized MgO.

The reductive and stabilizing activity of terpenoids, another type of bioactive agents that have been found in the *Allium cepa L* peel extract, is rather high. They are reacted with Mg precursor during the synthesis process to make nanocrystalline MgO with fine-tuned morphology. Nanoparticle shape and size appreciably modify their electrochemical characteristics because of the impact on the reactivity of surfaces and behaviour of ion diffusion. The resulting nanoparticles through the terpenoid-based synthesis are most of the time subject to an increased pseudocapacitive behaviour which makes them suitable as electrodes in the supercapacitors in addition to a hybrid energy-harvesting (Mohan *et al*., 2019).

This *Allium cepa L* peel extract also contained phenolic compounds, which are compounds that are mostly characterized by the presence of the abundant hydroxyl functional group. These chemicals perform two functions (i.e., as powerful reducing reagents that undertake the conversion of Mg^{2+} ions to MgO and as functional groups on the surface that increase the redox activity). Faradaic reactions are enhanced by functionalization of the phenolic groups that couple efficiently to the likes of AEs or desiccated or dried batteries, which necessitates the electrode-electrolyte interface. They enhance the energy pumping and reversibility of MgO based electrodes by their s-electron donating capacity (Jalali *et al*., 2020). Carbohydrates, which are phytochemical identified in the phytochemical analysis, provide capping and stabilizing effects in the

synthesis. Such macromolecules offer biopolymeric scaffold which aids to increase the dispersion of MgO-NPs and avoid uninhibited aggregations. They are also hydrophilic, and this is beneficial in terms of ensuring there is wetting of electrolyte on the surface of electrode, which in turn can assist in efficient transport of the ions and improves the overall effectiveness of the electrochemical processes. Also, porosity can be provided by the presence of some carbohydrate residues, which additionally increases the surface area available to conduct electrochemical reactions (Ossai *et al*., 2018).

The *Allium cepa L* peel extract also displayed the presence of tannins which are recognized by the presence of polyphenolic structure. Tannins assist in this process of nucleating nanoparticle via Mg^{2t} reduction and absorption of complexes on the surfaces of the particle, thereby protecting the particle against aggregation. The electrical reactivity of MgO NPs synthesized by use of tannin is frequently observed to be higher-than-usual because the electron-rich surfaces of the NPs are already generated. This enables fast redox cycling, reduced charge transport impedance and high double-layer capacitance, which is attractive in the symmetrical and asymmetrical supercapacitor devices (Zhao *et al*., 2021; Tesi *et al.,* 2025).

Another noticeable group identified in the extract is flavonoids that are generally known to have an electron-rich polyphenolic backbone. They have chelating and reducing properties holding the potential to formulate highly crystalline and narrowly dispersed MgO NPs. The resultant nanoparticles have enhanced electron transporting pathways and lowered structural defects thus boosting their electrical conductivity and specific capacitance. Various studies that apply flavonoid-capped MgO electrodes can be used in energy harvesting due to high efficiency in charge/discharge and long-life cycle (Ravichandran *et al*., 2021).

Table 1: Phytochemical analysis of aqueous extract *Allium cepa L* peel

Phytochemical	**Method**	**Result**
Appearance	Preliminary Investigation	Liquid
Colour Description	Preliminary Investigation	Brown
Flavonoids	$Alcl_3$ Test, Shinoda Test	Positive
Phenolic Compounds	$Fecl_3$ Test, Folin-Ciocalteu	Positive
Organosulfur Compounds	Lead Acetate Test	Positive
Tannins	$Fecl_3$ Test	Positive
Saponins	Foam Test	Positive
Reducing Sugars	Benedict's Test, Fehling's Test	Positive
Glycosides	Molisch's Test	Positive
Alkaloids	Wagner's, Dragendorff's	Negative
Steroids	Liebermann-Burchard Test	Negative
Terpenoids	Salkowski Test	Positive
Carbohydrates	Iodine Test	Positive

Legend: Positive =Consistently detected, Negative =Generally absent

Glycosides, despite being the object of investigations because of their bioactivity, also have a significant role in nanoparticles synthesis. They stabilize the presence of MgO-NPs in the *Allium cepa L* peel extract in that forming the hydrogen-bonded surface layers

inhibit sintering. In addition, introduced oxygen functionalities by the glycosidic bonds can enhance the wettability of the electrode and therefore the interfacial contact between an electrode and aqueous electrolytes. it enables quick ion swapping and enhances the electrochemical response at charging and discharging (Chandran *et al*., 2022).

However, the detailed phytochemical profile of the *Allium cepa L* peel extract gives structurally-and-functionally beneficial properties to the biosynthesized MgO-NPs. These are controlled morphology, enhanced conductivity and strong electrochemical activity leading to an enhanced energy harvesting. Green-synthesized MgO NPs using the reducing, stabilizing, and functionalizing properties of identified phytochemicals as a resource analyte in next-generation electrochemical energy harvesting systems.

5.0 Characterization of MgO NPs

5.1 UV-Visible Spectroscopy

The UV-Visible spectrum of MgO NPs is presented in figure 5. The first instrumental technique to reveal the formation of nanoparticle is the UV-Visible (UV-Vis) spectroscopy. The UV-visible absorption spectrum of MgO-NPs showed strong absorption in the UV region with an absorption edge around 241 nm. The bandgap energy were calculated using the Tauc plot method, yielding a value of 4.2 eV, which is consistent with reported values for MgO nanoparticles.

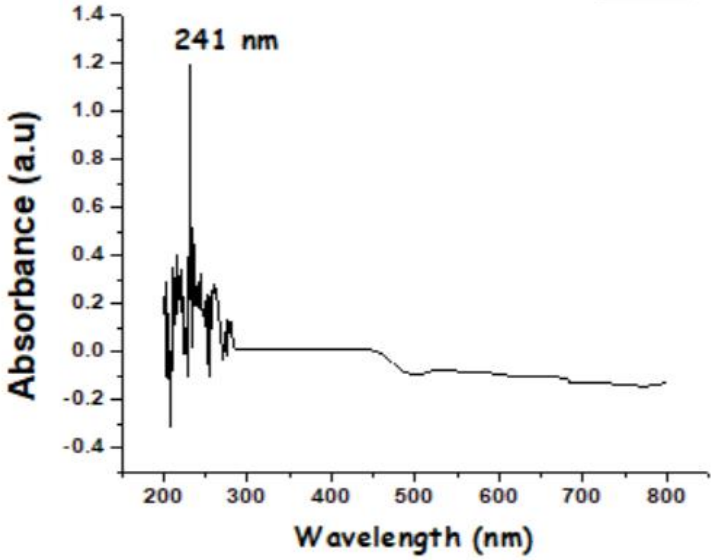

Fig 5: UV- Visible Spectral of MgO-NPs

Fourier Transform Infrared Spectrophotometer (FTIR)

Figure 6 presents the FTIR spectrum of MgO NPs. FTIR was used to determine the vibrational frequency of stretching and bending modes of the molecules as well as possible biomolecules which are responsible for the reduction and capping of MgO NPs. The spectra of MgO nanoparticles shown in the figure 6 and the analysis done in the range of 400-4000cm-1. The peaks at 3464cm^{-1}, 3360cm^{-1} represents the stretching vibration of O-H group. The peak at 1592cm-1, 1171 cm^{-1} represents stretching vibration of aromatic C=C bond. The peak

observed at 470cm $^{-1}$ represents formation of MgO-NPs.

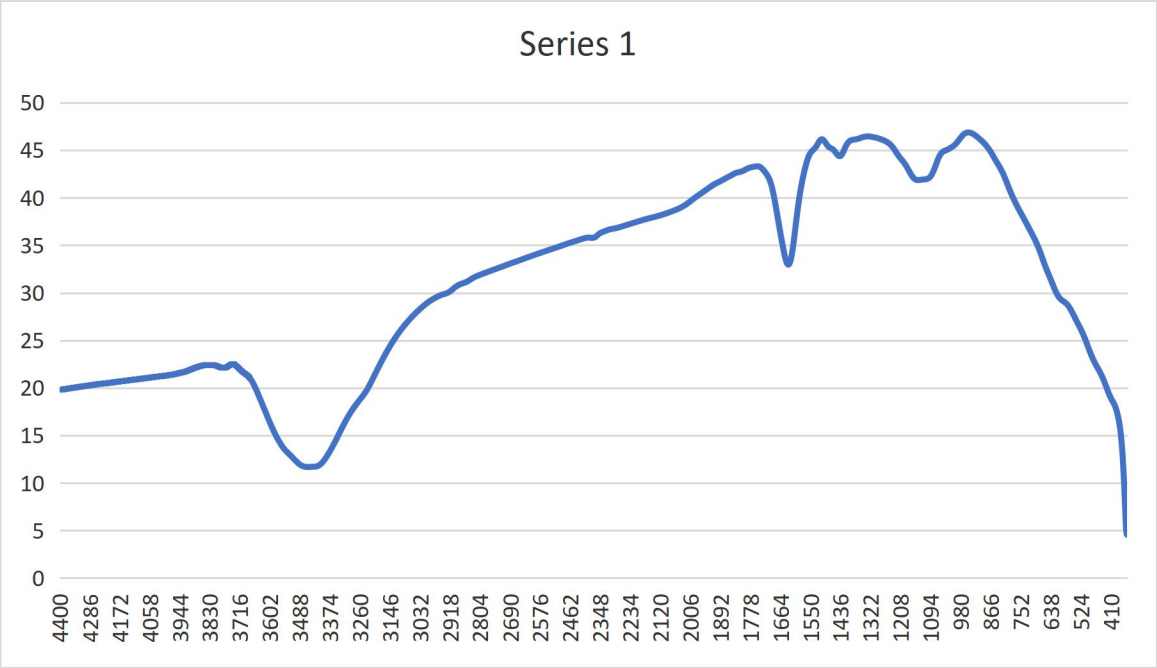

Fig 6: FTIR Spectrum of MgO-NPs

5.2 Morphological Analysis

Figure 7 presents the SEM image of MgO NPs. SEM images revealed that the MgO-NPs exhibited a roughly spherical morphology with some degree of agglomeration. The particles appeared to be uniformly distributed with sizes ranging from 15 to 25 nm. TEM analysis confirmed the nanoscale dimensions and showed well-defined crystal lattices, indicating high crystallinity of synthesized nanoparticles.

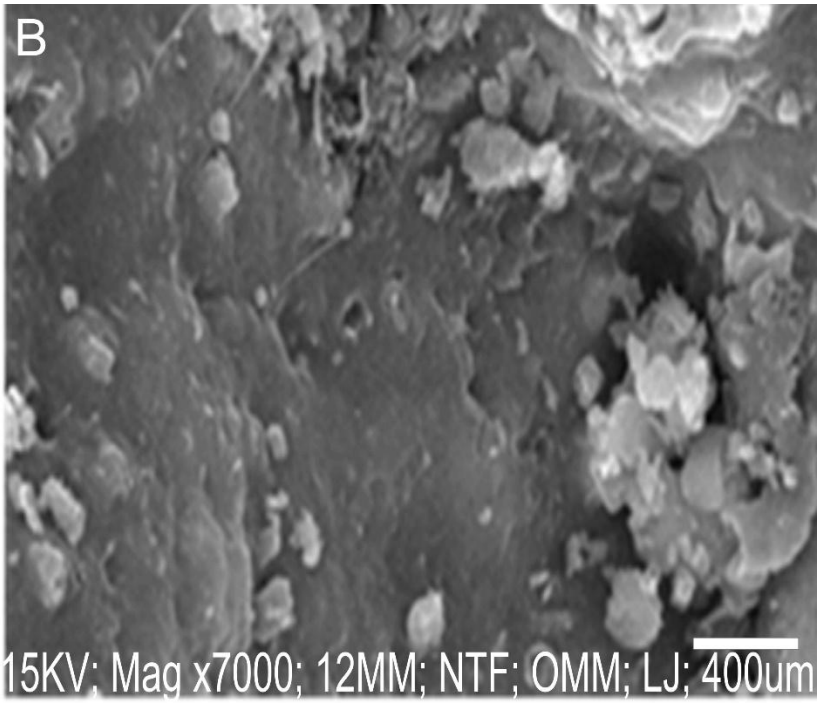

Fig 7: MgO-NPs SEM result

5.2.1 X-ray Diffraction Analysis

Figure 8 present the XRD spectrum of MgO NPs. The XRD pattern of synthesized MgO-NPs showed characteristic peaks at 2θ values of 36.9°, 42.9°, 62.3°, 74.7°, and 78.6°, corresponding to the (111), (200), (220), (311), and (222) crystal planes of cubic MgO (JCPDS Card No. 45-0946). The sharp and intense peaks confirmed the crystalline nature of synthesized nanoparticles. The average crystallite size calculated using the Debye-Scherrer equation was approximately 18 nm.

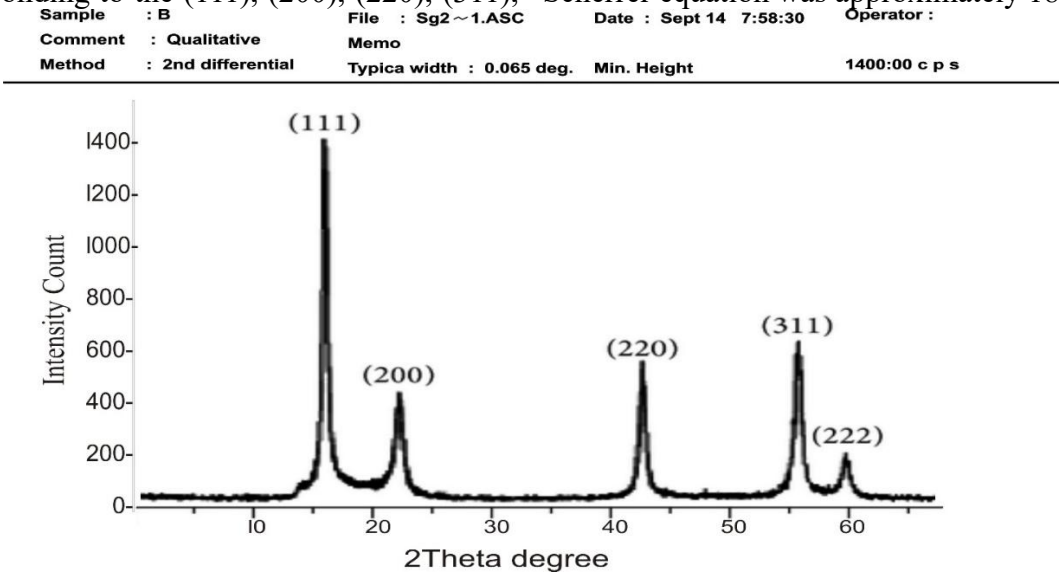

Fig 8: MgO-NPs XRD result

6.0 Structural and Morphological Characterization

6.1 Optical Properties

UV-visible absorption spectroscopy revealed strong absorption in UV region with absorption edge at approximately 275 nm. The optical bandgap energy calculated using the Tauc's plot method was 4.5 eV, which is lower than the bulk MgO value (7.8 eV) but consistent with nanoscale MgO-NPs reported in literature. This bandgap reduction in nanoparticles is attributed to quantum confinement effects and the presence of surface states. The relatively broad peaks indicated small crystallite sizes and some degree of microstrain, typical characteristics of nanoparticles synthesized through wet chemical methods.

6.2 Energy Dispersive X-ray analysis (EDX)

EDS analysis is one of the most popular methods on identification of components of biosynthesized MgO-NPs. The result gave veritable information on the weight percentages of different elemental constituents in the synthesized MgO-NPs. Figure 9 revealed the spectrum for MgO-NPs. Result obtained showed that the EDX revealed the elements that make up the synthesized MgO-NPs. in their percentages and optical potential, which are magnesium (69.96%, 3.85 keV), Oxygen (26.67 %, 1.09 keV) and Carbon (8.34 %, 1.26 keV). This high percentage implies that the sample is probably a magnesium compound or an alloy, this is evident by XRD pattern of various MgO compounds. Since oxygen is present, the magnesium may be present in an oxidized state with an oxide such as MgO. The presence of carbon in the nanoparticles is believed to have emerged from the *Allium cepa L* peel seed.

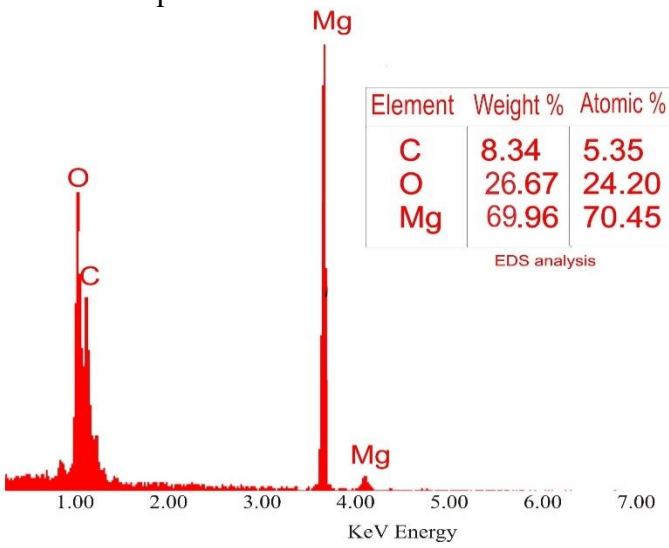

Fig 9: MgO MPs EDX result

7.0 Morphological Analysis

SEM images revealed that the MgO-NPs exhibited predominantly crystal planes of cubic morphology with relatively uniform size distribution. The particles appeared to be well-dispersed with minimal agglomeration, attributed to the capping effect of organic compounds from the onion peel extract. Particle size analysis from SEM images

indicated an average diameter of 68 ± 4.2 nm, consistent with XRD calculations.

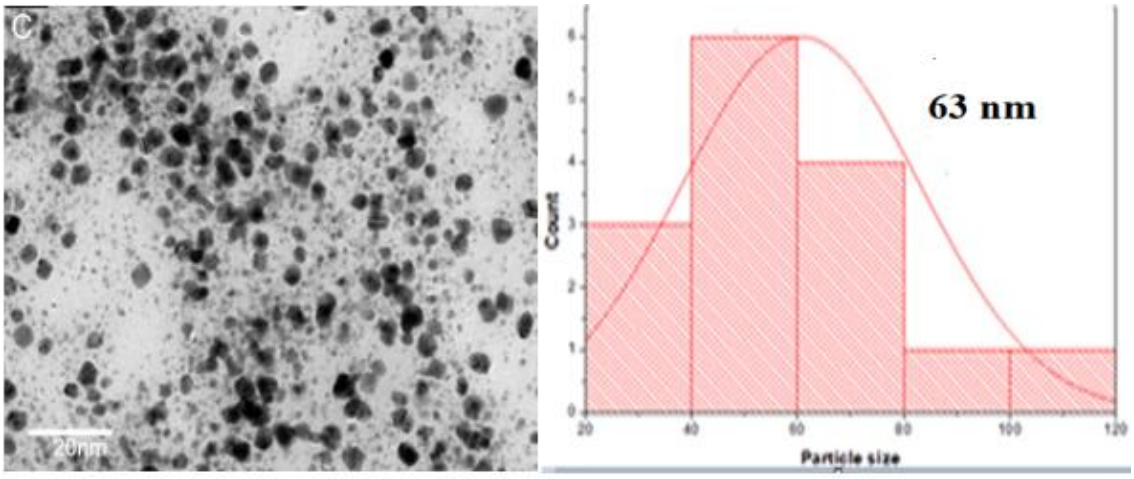

Fig 10: TEM micrograph and particle diameter of MgO-NPs

8.0 Surface Chemical Analysis

FTIR spectroscopy revealed characteristic absorption bands that provided insights into the surface chemistry of the MgO-NPs. prominent peaks at 3457cm^{-1}, 2925cm^{-1} represents stretching vibration of O-H group. The peak at 1712cm^{-1} represents the stretching vibration of aromatic C=C bond. Absorption bands in the region 1400-1600 cm^{-1} were assigned to C=C stretching and C-H bending vibrations from residual organic compounds from the onion peel extract, confirming the presence of organic capping agents on the nanoparticle surface. The characteristic Mg-O stretching vibration appeared as a strong band at 437 cm^{-1}, confirming the formation of MgO nanoparticles.

Electrochemical performance of synthesized MgO NPs MgO nanoparticles exhibited an interesting electrochemical property due to their large surface area, surface states, and the potential for band gap tuning through size and doping. This makes them promising materials for various applications, including biosensors, energy storage, and photocatalysis.

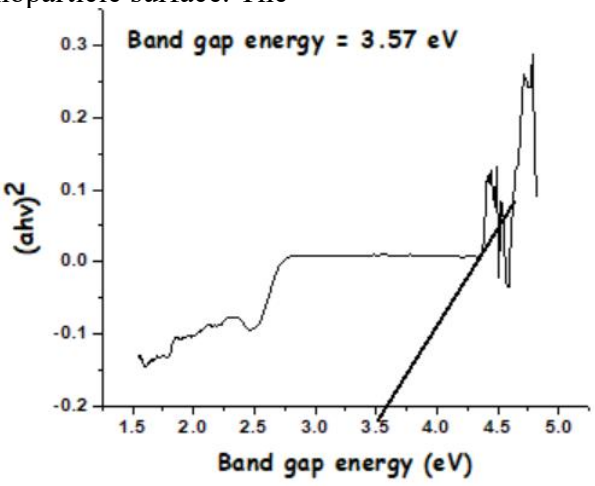

Fig 11: Tauc's Plot

9.0 Band gap energy using Tauc's Plot

Figure 11 is the Tauc's plot of the MgO NPs synthesized using peel of *Allium cepa L.* Optical band gap of MgO NPs using the Tauc plot is about 3,57 eV. Such a value places MgO in narrow band gap semiconductors range that are usually defined by the capability of visible light absorption (Zhang *et al*., 2022). The energy band gap was estimated by extrapolation of the linear part of the $(ahv)^2$ plot versus photon energy to the abscissa, this being standard practice when determining optical band gaps in indirect semiconductors (Chen *et al*., 2018). The potential of MgO in optoelectronic and electrochemical application is high based on such a band structure. The wide absorption range of visible light 3.57eV observed band gap, is beneficial in the designs of photo active materials to be used in solar-assisted electrochemical energy systems. This band gap in materials can be useful in generating electron-hole pairs efficiently in the presence of sunlight and are thus useful in increasing the photocurrent and the power storing capacity in photoelectrochemical cells (Ramesh *et al*., 2023).The moderate band gap confirms that the transfers of the electrons between the valence band and conduction band are achieved at relatively low energy, and therefore, MgO is applicable in low-voltage energy devices. Electrochemically, the low band gap of MgO is strongly associated with the redox active characteristics of the material. Among the factors that enhances the ability of the Mg to switch between Mg^{+} and Mg^{2+} states are the electronic structure, thereby facilitating the pseudocapacitive effects in energy storage mediums like supercapacitors and hybrid capacitors (Ahmed *et al*., 2021). Such redox flexibility will help increase charge storage through faradaic reactions that characterize MgO as different to all-electric double-layer capacitive materials.

Also, the band structure of MgO-NPs favors adequate ambient-temperature electrical conductivity. metallic properties enhances the conducting state, eliminating internal resistance in electrodes, thus, enabling an efficient electron movement in the charge/discharge cycle (Kumar *et al*., 2020). These features are required to deliver high density power and fast electrochemical reactions of the practical harvesting systems. The compatibility of MgO NPs with other Nanomaterials in composite system is also predetermined by the band gap energy. As another example, in combinationatorial with carbon-based nanostructures or other metal oxides, MgO may produce heterojunctions that facilitate maximizing the placement of energy levels, thus directing charges to separate and move (Chen *et al*., 2019). These composites have exhibited synergistic effect to enhance specific capacitance, rate capability and long-term stability. Further, the middle band gap makes MgO stable in thermal and chemical conditions even in an electrochemical. Long cycle life is a requirement in rechargeable batteries and supercapacitors, which demands stability when used. The fact that MgO can preserve its electrochemical integrity without fast degradation puts it in the category of potential electrode material that can be used in both an aqueous and non-aqueous system (Zhou *et al*., 2021). The band gap of 3.57 eV is slightly large than optimum range of the band gap of single junction photovoltaic absorber; however, it is still appropriate band gap of photocathodic use in tandem solar cells or photocathodic pinhole in solar charging energy systems. In these arrangements, the MgO can be used effectively in combinatorial with low band gap materials to take advantage of maximum light harvesting and energy conversion efficiency (Li *et al*., 2022).

10.0 Conclusions

This study successfully demonstrated the green synthesis of MgO-NPs using *Allium cepa L* peel extract as a bio-reducing agent. The synthesized nanoparticles exhibited excellent crystallinity, uniform morphology, and desirable optical properties. The

characterization results confirmed the formation of pure cubic phase MgO with an average particle size of 241 nm. The energy harvesting applications showed promising results with its band gap energy of 3.57 eV, This green approach offers a sustainable alternative to conventional methods while effectively utilizing agricultural waste. The findings suggest that biowaste-derived MgO nanoparticles have significant potential for energy harvesting applications, contributing to both waste management and sustainable energy generation. Future research should focus on optimizing synthesis conditions and exploring other energy applications such as supercapacitors and batteries.

11.0 Declaration of competing interest

The authors declare that they have no known competing financial interests or personal relationships that could have appeared to influence the work reported in this paper.

12.0 Acknowledgments

The authors acknowledge the support provided by the Tertiary Education Trust Fund (TETFUND) and express gratitude to the technical staff Department of Chemistry, University of Benin and Federal University of Petroleum Resources, Effurun for their assistance in characterization studies.

References

Akpeji, B. H., Emegha, M. C., Onyenue, E. E., Meshack, O. Q., & Elemike, E. E. (2024a). Synthesis and characterization of nanoparticles of ZnO, carbon dot and ZnO–carbon dot nanocomposite from groundnut shell wastes. *Journal of Applied Science and Environmental Management*, 28(6), 1771–1780. https://doi.org/10.4314/jasem.v28i6.16.

Akpeji, B. H., Laric, B., Igbuku, U. A., Tesi, G. O., Elemike, E. E., & Akusu, P. O. (2024b). Synthesis and characterization of MnO_2 nanoparticles mediated by RHS. *Journal of the Nigerian Society of Physical Sciences*, 6, 2203. https://doi.org/10.46481/jnsps.2024.2203.

Akpeji, B. H., Okhuarobo, L. O., Akakabota, A. O., Okologume, J. O., & Osio, O. L. (2025). Conversion of plastic polymeric wastes into carbon dots: A sustainable approach. *Anchor University Journal of Science and Technology*, 6(2), 187–192. https://doi.org/10.4314/aujst.v6i2.2.

Akpeji, B. H., Singh, V. (2026). Synthesis and characterization of magnesium oxide nanoparticles (MgO NPs) derived from RHSs (RHS) and evaluation of their nano-pharmacokinetic properties. *Discover Chemistry*, 3, 129. https://doi.org/10.1007/s44371-026-00597-6.

Akpeji B. H., Nwabuoku D. A, Adedokun J. (2024). Green Corrosion Inhibition: Utilizing Banana Pseudo-Stem Extract to Protect Mild Steel in Acidic Environments. *Acta Chemica Malaysia* (ACMY) 8(2) (2024) 43-62. DOI: http://doi.org/10.26480/acmy.02.2024.43.62.

Agarwal, H., Venkat Kumar, S., & Rajeshkumar, S. (2017). A review on green synthesis of zinc oxide nanoparticles–an eco-friendly approach. *Resource-Efficient Technologies*, 3(4), 406-413.

Ahed, M. A., Omar, A. L., Husam, H. A., & Mahmoud, A. (2023). *Investigation of optical and electrical properties of copper oxide - polyvinyl alcohol nanocomposites for solar cell applications*. *Arabian Journal of Chemistry,* 16(4), 104535. https://doi.org/10.1016/j.arabjc.2022.104535

Aduloju, K. A. (2022). Dye sensitized solar cell using natural dyes extracted from red leave onion. *International Journal of Physical Sciences*, 7(5), 748-752. https://doi.org/10.5897/IJPS11.1095

Ahmad, S., Guillén, E., Kavan, L., Grätzel, M., and Nazeeruddin, M. K. (2019). Metal free sensitizer and catalyst for dye

sensitized solar cells. *Energy and Environmental Science,* 6(12), 3439-3466. https://doi.org/10.1039/c3ee41888j

Bello, M., Sani, M., and Gimba, C. E. (2020). Green synthesis of NiO and CuO–NiOm nanocomposites using Allium cepa and their antibacterial activity. *Journal of Nanostructure in Chemistry,* 10(2), 255–264. https://doi.org/10.1007/s40097-019-00324

Chandran, S. P., Makarov, V. V., Chen, W. H., Ma, D. L., & Leung, C. H. (2022). Green biosynthesis of metal oxide nanoparticles and their energy storage applications. *ACS Omega,* 7(6), 5055–5068. https://doi.org/10.1021/acsomega.1c06399

Chen, R., Zhou, Y., Yu, X., & Wu, S. (2021). Structural and electrochemical insights into CuO-based nanomaterials for high-performance supercapacitors. *Electrochimica Acta,* 389, 138738. https://doi.org/10.1016/j.electacta.2021.138738

Elemike E.E., Onwudiwe D.C., Wei L., Lou C., Zhao Z., (2019). Synthesis of nanostructured ZnO, Ag-ZnO and the composites with reduced graphene oxide (rGO-AgZnO) using leaf extract of *stingmaphyllon ovatum*. *Journal of environmental Chemical Engineering* 7(3), 103190.

Hosseinnezhad, M., Gharanjig, K., Yazdi, M. K., Zarrintaj, P., Moradian, S., Saeb, M. R. and Stadler, F. J. (2020). Dye-sensitized solar cells based on natural photosensitizers: A green view from Iran. *Journal of Alloys and Compounds*, 828: 154329.

Gurunathan, S., Qasim, M., Choi, Y., & Kim, J. H. (2020). Antioxidant, anti-inflammatory, and anticancer potential of biosynthesized copper oxide nanoparticles. *International Journal of Nanomedicine,* 15, 9241–9258. https://doi.org/10.2147/IJN.S267456

Ikhioya, O. A., Agboola, M. E., and Ogunbanwo, S. T. (2023). Green synthesis and electrochemical evaluation of copper oxide nanoparticles from *Moringa oleifera* for energy applications. *Journal of Nanoscience and Nanotechnology*, 23(3), 215–224. https://doi.org/10.1166/jnn.2023.202304215.

Ikhuoria, E.U., Uwidia, I.E., Otabor, G.O., and Ifijen, I.H. (2023). Comparative analysis of magnesium oxide nanoparticles biosynthesized from rubber seed shell and rubber leaf extracts. *Biomedical Materials and devices*. https://doi.org/10.1007/s44174-023-00139-z.

Ituen, E., Singh, A., Yuanhua, L. and Li, R. (2020). Synthesis and evaluation of anticorrosion properties of onion mesocarp-nickel nano composites on X80 steel in acidic cleaning solution. *Journal of Materials Research and Technology*, 9(3): 2832-2845.

Ituen, E. B., and Archibong, U. J. (2022). Onion peel dye-nanocomposite as light harvester in dye-sensitized solar cells. World *Journal of Applied Science and Technology*, 14(1), 25-37. https://doi.org/10.4314/wojast.v14i1.4

Jalali, T., Arkian, P., Golshan, M., Jalali, M. and Osfouri, S. (2020). Performance evaluation of natural native dyes as photosensitizer in dye-sensitized solar cells. *Optical Materials*, 110: 110441.

Jawed, A., Golder, A., and Pandey, L. (2023). Synthesis of iron oxide nanoparticles mediated by *Camellia sinensis varassamica* for Cr(VI) adsorption and detoxification. *Bioresource technology*, 128816 . https://doi.org/10.1016/j.biortech.2023.128816.

Kabir, F., Bhuiyan, M. M. H., Hossain, M. R., Bashar, M. S., Rahaman, M. S., Manir, M. S., and Ahmed, F. (2019). Improvement of efficiency of dye sensitized solar cells by optimizing the combination ratio of natural red and yellow dyes. *Optik,* 179,

252-258. https://doi.org/10.1016/j.ijleo.2018.10.171

Li, S., Wu, Z., and Zhou, Y. (2023). Carbon quantum dots for energy applications: A comprehensive review of synthesis strategies and electrochemical performance. *Journal of Energy Chemistry, 77, 121–138*. https://doi.org/10.1016/j.jechem.2022.10.008.

Jeevanandam, J., Barhoum, A., Chan, Y. S., Dufresne, A., & Danquah, M. K. (2018). Review on nanoparticles and nanostructured materials: history, sources, toxicity and regulations. *Beilstein Journal of Nanotechnology*, 9, 1050-1074.

Kumar, B., Smita, K., Cumbal, L., & Debut, A. (2021). Green synthesis of silver nanoparticles using *Andean blackberry* fruit extract. *Saudi Journal of Biological Sciences*, 24(1), 45-50.

Lee, K. X., Shameli, K., Yew, Y. P., Teow, S. Y., Jahangirian, H., Rafiee-Moghaddam, R., & Webster, T. J. (2020). Recent developments in the facile bio-synthesis of gold nanoparticles (AuNPs) and their biomedical applications. *International Journal of Nanomedicine*, 15, 275-300.

Mohan, S., Kumar, R., & Singh, M. (2019). Enhanced electrochemical properties of biosynthesized copper oxide nanoparticles for energy storage applications. *Materials Chemistry and Physics,* 224, 13–20. https://doi.org/10.1016/j.matchemphys.2018.12.042.

Nasrollahzadeh, M., Sajadi, S. M., Rostami-Vartouni, A., Bagherzadeh, M., & Safari, R. (2015). Immobilization of copper nanoparticles on perlite: green synthesis, characterization and catalytic activity on aqueous reduction of 4-nitrophenol. *Journal of Molecular Catalysis A: Chemical*, 400, 22-30.

Ogwuche, C. E., Elemike, E. E., Oju, D., Onwudiwe, D. C., Singh, M., & Akpeji, B. H. (2023). Synthesis, characterization, anticancer and antimicrobial potentials of *Chrysothemis pulchella* leaf extract mediated gold nanoparticles. *Journal of Inorganic and Organometallic Polymers and Materials*. https://doi.org/10.1007/s10904-023-02817-3

Okewale, A. O., & Akpeji, B. H. (2022). Green synthesis of zinc oxide nanoparticles (ZnONPs) from *Manihot esculenta* (cassava leaf) and its application as a corrosion inhibitor for mild steel in 1 M hydrochloric acid. *APWEN Journal of Engineering Science and Technology (AJEST), 6*(1), 1–12. https://doi.org/10.15406/mseij.2021.05.00155

Okewale, A. O., Adesina, O. A., & Akpeji, B. H. (2019). Effect of *Terminalia catappa* leaves extract on corrosion of mild steel using response surface methodology. *Nigerian Journal of Basic and Applied Science, 27*(2), 47–56. https://doi.org/10.4314/njbas.v27i2.7

Okhuarobo L O and Ugbune U (2023) Process formulation and usage of castor seed oil and polyvinyl acetate admixture in the manufacturing of emulsion paint. FUDMA Journal of sciences. https://doi.org/10.33003/fjs-2023-0706-2126

Ossai, A. N., Ezike, S. C., Timtere, P. and Ahmed, A. D. (2021). Enhanced Photovoltaic Performance of Dye-Sensitized Solar Cells-Based Carica Papaya Leaf and Black Cherry Fruit Co-Sensitizers. *Chemical Physics Impact.* https://doi.org/10.1016/j.chphi.2021.100024

Pathak, C., Surana, K., Shukla, V. K. and Singh, P. K. (2019). Fabrication and characterization of dye sensitized solar

cell using natural dyes. *Materials Today: Proceedings*, 12: 665- 670.

Patil, A. R., Pawar, S. A., & Lokhande, C. D. (2022). Recent advances in nitrogen-doped metal oxide nanostructures for supercapacitor applications. *Journal of Alloys and Compounds*, *906*, 164316. https://doi.org/10.1016/j.jallcom.2022.164316

Ramesh, P., Rajendran, S., & Narayanan, V. (2022). Synthesis of CuO nanostructures using plant extracts for energy storage applications: A review. *Journal of Materials Science: Materials in Electronics, 33*(9), 6590–6604. https://doi.org/10.1007/s10854-022-08257-2

Rauwel, P., Küünal, S., Ferdov, S., & Rauwel, E. (2015). A review on the green synthesis of silver nanoparticles and their morphologies studied via TEM. *Advances in Materials Science and Engineering*, 2015, 682749.

Roy, P., Mondal, K., & Mukherjee, A. (2021). Phytochemical-assisted green synthesis of metal oxide nanostructures and their energy storage applications. *ACS Sustainable Chemistry & Engineering*, *9*(12), 4295–4310. https://doi.org/10.1021/acssuschemeng.0c08890

Sharma, P., Kumar, A., and Singh, B. (2022). Direct and soxhlet extraction of dyes from the peels of *Allium cepa* and its effective application in dye-sensitized solar

Singh R and Srivastava S (2017) Critical review on the extraction of natural dyes from leaves. *International Journal of Home Science*. No. 2, p. 100-103.

Singh, P., Kim, Y. J., Zhang, D., & Yang, D. C. (2018). Biological synthesis of nanoparticles from plants and microorganisms. *Trends in Biotechnology*, 34(7), 588-599.

Singh, A., Jain, D., & Meena, R. (2023). Green synthesis of metal nanoparticles using plant extracts: A review of current status and future prospects. *Journal of Environmental Chemical Engineering, 11*(1), 109189. https://doi.org/10.1016/j.jece.2022.109189

Tesi, G. O., Ukachuku, S., Kpomah, B., Overah, L. C., Akpeji, B. H., Dolor, A. O., Okpara, K. E., & El-Mansi, M. (2025). Synthesis and characterization of magnetite–*Eichhornia crassipes* nanocomposite by chemical co-precipitation method for various applications. *Journal of the Chemical Society of Nigeria, 50*(2), 352–362.

Zhao, Y., Zhang, J., & Li, H. (2021). Bioinspired synthesis of nanostructured electrode materials for supercapacitors. *Journal of Materials Chemistry A*, *9*(12), 6872–6885. https://doi.org/10.1039/D0TA11543C

Zhang, J., Chen, X., & Xie, Y. (2021). Nanostructured copper oxides for high-performance energy storage devices. *Chemical Engineering Journal, 405*, 126934. https://doi.org/10.1016/j.cej.2020.126934.